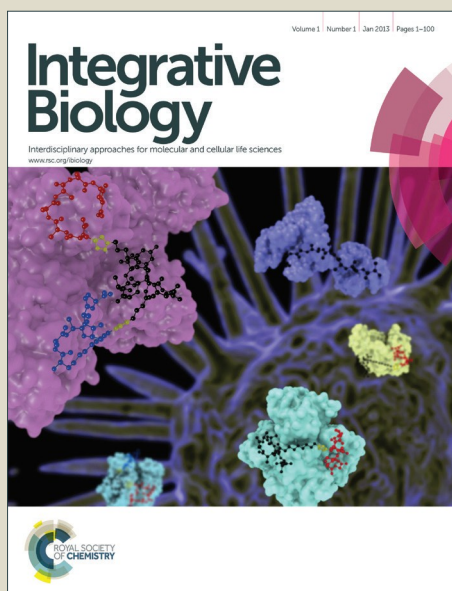


Integrative Biology

Accepted Manuscript



This is an *Accepted Manuscript*, which has been through the Royal Society of Chemistry peer review process and has been accepted for publication.

Accepted Manuscripts are published online shortly after acceptance, before technical editing, formatting and proof reading. Using this free service, authors can make their results available to the community, in citable form, before we publish the edited article. We will replace this *Accepted Manuscript* with the edited and formatted *Advance Article* as soon as it is available.

You can find more information about *Accepted Manuscripts* in the [Information for Authors](#).

Please note that technical editing may introduce minor changes to the text and/or graphics, which may alter content. The journal's standard [Terms & Conditions](#) and the [Ethical guidelines](#) still apply. In no event shall the Royal Society of Chemistry be held responsible for any errors or omissions in this *Accepted Manuscript* or any consequences arising from the use of any information it contains.

Insight, Innovation, Integration

Endocytosis is a critical process in cellular signaling and homeostasis and continuously adapts to the physiological state of a cell. We present a quantitative analysis of how physical cues, specifically cell spreading area, alter the dynamics of clathrin-coated pits (CCPs). As a technological innovation, we combined microcontact printing with live single cell imaging and high content image analysis to investigate CCP dynamics under controlled cell size and shape. These studies led to the biological insight that cell spreading area and the presence of the actin cortical network, acting possibly through tension, could alter dynamic properties of CCPs. We further discovered that cortical contractility influences CCP growth. Novel aspects of cell mechanotransduction are observed by integrating a controlled physical microenvironment with quantitative live cell imaging.

Cell Spreading Area Regulates Clathrin-Coated Pit Dynamics on Micropatterned Substrate

Xinyu Tan¹, Johanna Heureaux¹, Allen P. Liu^{1,2,3,4,*}

¹ Department of Mechanical Engineering, University of Michigan, Ann Arbor, Michigan, United States of America, ² Department of Biomedical Engineering, University of Michigan, Ann Arbor, Michigan, United States of America, ³ Cellular and Molecular Biology Program, University of Michigan, Ann Arbor, Michigan, United States of America, ⁴ Biophysics Program, University of Michigan, Ann Arbor, Michigan, United States of America.

* Corresponding author: Allen P. Liu, Ph.D., University of Michigan, Ann Arbor, 2350 Hayward Street, MI 48105. Tel: 734-764-7719, Email: allenliu@umich.edu

Abbreviations used: CME: clathrin-mediated endocytosis; CCP: clathrin-coated pits; PDMS: polydimethylsiloxane;

Abstract

Clathrin-mediated endocytosis (CME) is the most characterized pathway for the endocytic entry of proteins and lipids at the plasma membrane of eukaryotic cells. Numerous studies have probed the roles of different endocytic accessory proteins in regulating the dynamics of clathrin-coated pit (CCP) assembly. However, it is not completely clear how physical cues regulate CCP dynamics. Here we employ microcontact printing to control cell shape and examine CCP dynamics as a function of cell spreading area for three differently sized cells. Cells with a large spreading area had more short-lived CCPs but a higher CCP initiation rate. Interestingly, we found that fluorescence intensity of CCPs decreased with increasing cell spreading area in a manner that was dependent on the cortical actin network. Our results point to another facet of the regulation of CCP dynamics, suggesting that CME may be modulated while cells change their mechanical state and remodel their actin cytoskeleton during various processes.

Insight, Innovation, Integration

Endocytosis is a critical process in cellular signaling and homeostasis and continuously adapts to the physiological state of a cell. We present a quantitative analysis of how physical cues, specifically cell spreading area, alter the dynamics of clathrin-coated pits (CCPs). As a technological innovation, we combined microcontact printing with live single cell imaging and high content image analysis to investigate CCP dynamics under controlled cell size and shape. These studies led to the biological insight that cell spreading area and the presence of the actin cortical network, acting possibly through tension, could alter dynamic properties of CCPs. We further discovered that cortical contractility influences CCP growth. Novel aspects of cell mechanotransduction are observed by integrating a controlled physical microenvironment with quantitative live cell imaging.

Introduction

Clathrin-mediated endocytosis (CME), a major and robust pathway through which many nutrient molecules and receptors are internalized in eukaryotic cells, occurs constitutively on the plasma membrane through the functional unit: clathrin-coated pits (CCPs). As CME regulates cell surface expression of signaling receptors, it plays a role in organismal physiology in development, health, and disease. A large number of accessory proteins together with cargo, adaptors, and clathrin help orchestrate the initiation, assembly, and invagination of CCPs¹. Live cell imaging studies have facilitated the observation of the dynamics of individual molecular components with spatial and temporal details and revealed distinct dynamics through the quantification of CCP lifetime, initiation and intensity²⁻¹⁰. These studies have shown how cargo, lipids, adaptor and accessory proteins could regulate CCP dynamics in a variety of experimental cell systems. However, the impact of physical and mechanical cues on CCP dynamics, and therefore CME, is relatively less understood.

From earlier work, it is well appreciated that membrane physical properties and trafficking are closely related¹¹. During cell spreading, a burst of exocytosis is activated due to the sudden increase in membrane tension¹². Early evidence showed that the uptake of transferrin, a canonical cargo for CME, was inhibited during mitosis¹³ during which a cell exhibits large membrane tension. Caveolae, which are functional units of caveolae-mediated endocytosis, rapidly disassemble upon acute mechanical stress such as hypo-osmotic shock or uniaxial stretching, which both increase membrane tension¹⁴.

Clathrin-coated structures can respond to changes in membrane tension such that actin polymerization becomes a requirement for internalization. In yeast, CME is constitutively actin dependent. By changing osmolarity, it was found that turgor pressure is important for robust formation of an actin network during endocytosis and subsequent pressure alleviation resulted in endocytosis in the absence of an actin network¹⁵. In mammalian cells, actin polymerization is

usually dispensable for CME¹⁶. Using polarized epithelial cells that display high membrane tension on the apical side and low membrane tension on the basolateral side, Boulant et al. showed that actin dynamics works against membrane tension to invaginate the membrane to form a CCP¹⁷. At high membrane tension, actin engagement was necessary for CCP internalization, and this requirement can be recapitulated in cells that underwent osmotic swelling or mechanical stretching.

Using a subcellular-sized pattern of extracellular matrix proteins to control the spatial organization of focal adhesions, we previously found that CCP lifetimes were significantly longer in the patterned regions that had higher cortical actin density¹⁸. Subcellular patterning controls focal adhesion assembly and organization and in effect generates an atypical cytoskeletal phenotype. Reduction of cortical actin abolished the increase in CCP lifetime, suggesting that the observed CCP lifetime changes could be controlled by cell morphology on these subcellular patterned substrates. The atypical cytoskeleton structure likely has a strong effect on the traction stresses exerted on the substrate and hence produced the local effects that were observed.

At the cellular level, controlling the degree of cell spreading has a large effect on cellular processes such as growth, death, and differentiation^{19,20}. Unfortunately, we only know that controlling sub-cellular focal adhesion patterns is capable of modifying CME and CCP dynamics. Therefore, we set out to determine if spatial confinement, at the cellular level, is capable of altering CCP dynamics in distinct ways to better understand how cell shape alters cell physiology.

In this study, we employed microcontact printing of cell-sized pattern to control the degree of cell spreading. Combining this microfabrication tool with live-cell imaging and quantitative image analysis, we examined three aspects of CCP properties: lifetime distribution, initiation density, and CCP fluorescence intensity. We found that cells with larger spreading areas had more short-lived CCPs and a decrease in the maximum CCP fluorescence intensity.

Furthermore, we showed that actin depolymerization and inhibition of myosin contractility increased the maximum CCP fluorescence intensity. These results reveal a novel facet of how resting cell size, and the associated actin cortical network, can regulate CCP dynamics.

Materials and method

Cell lines and antibodies. Retinal pigment epithelial (RPE) cells are used in this study as they have been previously used for studying CCP dynamics²¹. RPE cells stably expressing enhanced green fluorescent protein tagged clathrin light chain a (EGFP-CLCa) were generated through infection with retroviruses in a pMIEG3 vector followed by FACS sorting^{5, 21} and maintained in Dulbecco's Modified Eagle Medium with nutrient mixture F-12 (DMEM/F-12; GIBCO, Grand Island, NY) supplemented with 10% (v/v) fetal bovine serum (FBS) (Sigma, St. Louis, MO) and 2.5% (v/v) penicillin/streptomycin (Invitrogen, Grand Island, NY) at 37 °C and 5% CO₂. Anti-paxillin and all secondary antibodies were used at a dilution of 1:1000 (Invitrogen), anti-YAP was used at a dilution of 1:200 (Cell Signaling Technology, Danvers, MA), and anti-alpha adaptin (AP6) for AP2 was used at a dilution of 3:1000 (Abcam, Cambridge, MA).

Microcontact printing. Standard soft lithography techniques were used to create the silicon master mold from which polydimethoxysiloxane (PDMS) stamps were made. PDMS stamps were prepared by mixing Sylgard-184 elastomer and curing agents (Dow Corning, Midland, MI) at a ratio of 10:1 to 20:1 (w/v), casting over the mold, and curing at 50 °C overnight. Inking solution made with 40 µg/ml fibronectin (Sigma) and 20 µg/ml Alexa Flour 647 fibrinogen (Invitrogen) was added to the PDMS stamps and incubated for 1 hour at room temperature. After excess inking solution was removed and the stamp washed with deionized water and blown dry with a stream of filtered air, the stamp was placed in conformal contact with a UV-ozone treated PDMS-coated coverslip for approximately 5 s. PDMS-coated coverslips were prepared by spin-coating a layer of PDMS diluted in hexane (1:20) at 5000 rpm for 2 min²².

resulted in a thickness of $72 \text{ nm} \pm 14 \text{ nm}$ ($n=4$) as measured by a profilometer. PDMS-coated coverslips were used to promote efficient transfer of stamped proteins. After stamping was completed, the PDMS-coated coverslip was passivated with 0.1% Pluronic-F127 (Sigma) for 1 hour, washed with PBS, and kept in PBS at $4 \text{ }^\circ\text{C}$ for no more than 3 days before use.

Immunofluorescence. Cells were permeabilized and fixed in 0.5% Triton X-100 (Sigma) and 2% paraformaldehyde (Electron Microscopy Sciences, Hatfield, PA) in PBS for 6 min followed by another 30 min fixation in 4% paraformaldehyde in PBS. Immunofluorescence images for were taken using either an Olympus-IX81 microscope with spinning disk confocal scanner unit (CSU-X1; Yokogawa, Japan), EMCCD camera (iXon X3; Andor, South Windsor, CT), 60x objective (NA = 1.42) or an Nikon A1 confocal system mounted on a Nikon Ti2000E inverted, fluorescence microscope with DIC optics (Nikon, Japan). To quantify YAP localization, we manually classified the cells into three groups according to the contrast of nuclear to cytosol intensity of YAP and then calculated the percentage of cells with the distinct nuclear or cytosol staining for each sized cells.

Live cell imaging via total internal reflection fluorescence (TIRF) microscopy. RPE cells expressing EGFP-CLCa were plated on microprinted surface at a low concentration and allowed to spread for 4 to 8 hours, and only individual cells that fully spread on the pattern were imaged. TIR-FM was performed on a Nikon TiE-Perfect Focus System (PFS) microscope equipped with an Apochromat 100x objective (NA 1.49), a sCMOS camera (Flash 4.0; Hamamatsu Photonics, Japan), and a laser launch controlled by an acousto-optic tunable filter (AOTF). Cells were imaged at 2 s intervals for 10 min at $37 \text{ }^\circ\text{C}$ in a home-made imaging chamber consisting of the coverslip with seeded cells mounted on a slide with two strips of double-sided tape used as spacers. PDMS has an intermediate refractive index between glass and water that permitted the evanescent wave to be produced at the PDMS-water interface²³. 25 nM latrunculin A (Fisher

Scientific, Pittsburg, PA) and 3 μM Y-27632 (Calbiochem, Billerica, MA) were applied to patterned cells and kept in the 37 °C incubator with 5 % CO_2 for 20 min before acquiring images. Imaging chamber was filled with the corresponding medium.

Image analysis for CCP dynamics. Image analysis was performed as described previously²⁴.

In brief, Gaussian mixture model fitting was used to detect and localize CCPs. Then, CCP tracking was performed using the μ -track package with a gap-closing feature, which generates trajectories of CCPs by linking the corresponding CCPs in consecutive frames. CCPs with lifetime less than 10 s were considered as transient structures and removed from later analysis. To further filter out the transient structures on the membrane, we also removed structures whose maximum intensity was below an intensity threshold, which was set from maximum intensity in the first 6 s of all the CCPs. We further calculated the proportion of CCPs at each lifetime from 10s to 600s for each group of cells to obtain the lifetime distribution, but only data for the 10s to 120s cohorts were plotted. Initiation density representing how frequent CCPs appear for a given unit area per unit time was calculated by dividing the median number of the newly appearing CCPs in each frame by the adhesive area of the cell and the interval (1/30 min). Intensity analysis was performed as described previously²⁵. CCPs were classified into six cohorts according to their lifetimes. Within each cohort, the procedure first realigned and averaged the first time point of intensity time course, yielding the “appearance-aligned” average. The time course was then aligned to the last time point and averaged, yielding the “disappearance-aligned” average. The global average was calculated as the weighted appearance and disappearance-aligned average, weighted towards appearance-aligned trace at the beginning and disappearance-aligned trace in the end. The plateau intensity was calculated as 95% of the maximum intensity values in the intensity profile of a cohort.

Statistical analysis. For lifetime distribution data sets, Komolgorov-Smirnov tests were performed to verify the statistical significance. For each data set, we first ran Anderson-Darling test for normality. For the data set that rejects the normality, Wilcoxon rank sum test was performed between that data set and the group which it compares with. Statistical difference of other data sets was determined by two-tailed Student's t test.

Results

Proportion of short-lived CCPs and initiation density increases with cell spreading area independent of cell shape

Microcontact printing was previously used to precisely control cell shape and the extent of cell spreading²⁰. We employed this technique to generate cell-sized fibronectin islands onto polydimethylsiloxane (PDMS)-coated coverslip via a PDMS stamp and blocked the surrounding areas with Pluronic F127 to prevent spreading of cells beyond the patterned areas (Figure 1A). Retinal pigment epithelial (RPE) cells stably expressing enhanced green fluorescent protein (EGFP) tagged to clathrin light chain a (CLCa) spread on circular fibronectin islands of 625 μm^2 , 1024 μm^2 and 2500 μm^2 . Average RPE cells spread to $\sim 1000 - 1200 \mu\text{m}^2$ on unpatterned substrates, so the sizes appropriately sample both above and below the average cell spreading area.

When cells were plated on these substrates, actin stress fibers were found to localize along the circumference of the cells with focal adhesions marked by the focal adhesion protein paxillin concentrated at the periphery of the cells (Figure 1B), forming fibrillar structures on larger cells. Actin filaments were much thicker and organized for the larger patterns (2500 μm^2), suggestive of a higher cytoskeletal stress developed in these cells similar to what was observed previously²⁶. CCPs, as imaged by confocal fluorescence microscopy, were found throughout the bottom surface of the cell.

To probe the dynamics of CCPs with different cell spreading areas, we combined time-

lapse live cell total internal reflection fluorescence (TIRF) imaging with single particle detection and tracking^{24, 27}. Three dynamic properties could be obtained from these time lapse movies: 1) Lifetime – defined as the time interval from CCP appearance to disappearance in the TIRF field, 2) Initiation density – defined as the number of CCP appearance per unit area and unit time, and 3) Fluorescence intensity of fluorescently tagged CLCa. We first determined the CCP lifetime distribution and compared the distributions among three different sizes of patterned cells. For cells that were more spread (2500 μm^2), there were more short-lived CCPs with lifetimes from 10 s to 18 s (Figure 1C). It has been suggested that CCPs with short lifetimes are likely to disassemble before getting internalized and are categorized as abortive CCPs^{2, 28}. Based on numerous work using a similar criterion^{24, 29-31}, we calculated the fraction of CCPs with lifetimes under 20 s for all cell areas. 29.1% of CCPs in 2500 μm^2 cells had lifetimes less than 20 s compared to 20.3% in 625 μm^2 ones (Figure 1C inset). Thus, in larger patterned cells, more short-lived CCPs, which presumably failed to internalize, were observed on the membrane.

We next asked whether cell spreading would alter CCP initiation. Cells on the largest pattern had an initiation frequency of $0.270 \pm 0.065 \mu\text{m}^{-2}\text{min}^{-1}$ for 2500 μm^2 cells compared to the smallest pattern $0.225 \pm 0.088 \mu\text{m}^{-2}\text{min}^{-1}$ for the 625 μm^2 cells (Figure 1D).

To test if the observed differential CCP dynamics was truly related to cell area, we also examined CCP dynamics on square fibronectin islands that had the same areas as the circular patterns (Figure 2A). Though cells on smaller islands (625 μm^2 and 1024 μm^2) still formed circumferential actin rings, 2500 μm^2 square cells formed distinct stress fibers (Figure 2B). Despite the differences in actin and focal adhesion organization between circular- and square-shaped cells, CCP dynamics followed the same trends. There were more short-lived CCPs along with a higher initiation density in the largest square cells (Figure 2C, D), confirming our results with circular patterned cells. This demonstrates that controlling cell spread area alone is sufficient to modulate CCP dynamics.

CCP fluorescence intensity is lower with larger cell spreading area due to a decreased rate of fluorescence change

To examine the effect of cell spreading on CCP intensity, we tracked the fluorescence intensity of the EGFP-tagged CLCa in CCPs imaged by TIRF microscopy over their lifetimes in 625 μm^2 , 1024 μm^2 and 2500 μm^2 patterned cells. Due to the wide distribution of CCP lifetimes, CCPs with lifetime ranges from 20 – 120 s were binned into six 20 s cohorts each with several thousands CCPs to obtain average trajectories in our analyses. The increase, plateau (i.e. maximum intensity), and the sudden decrease in intensity tracks of lifetime cohorts corresponded to the growth, maturation, and scission or disassembly of CCPs respectively (Figure 3A). Comparing the three different sizes of circular cells, we found that fluorescence intensity decreased as cell spreading area increased (Figure 3A). Average plateau intensity, which was defined as 95% level of the maximum intensity from the averaged intensities of each cohort, decreased with cell spreading in both circular and square cells (Figure 3B). In freely spreading cells which assumes various sizes and shapes, the average plateau intensity was also lower for larger cells (Figure 3C), consistent with our results from the patterned substrates.

To exclude the possibility that the exponential decay of the excitation field with the distance away from the glass-aqueous interface in TIRF imaging affected our result, we used spinning disk confocal microscopy, which has a constant excitation power over the depth of focus (~500 nm). These experiments showed the same results as with our live cell TIRF measurements and confirmed that the intensity of CCPs decreased with increasing cell spreading area in fixed cells (Supplemental Figure S1A). Since CLCa incorporation in clathrin triskelia is not critical for endocytosis³², it is possible that our results can be explained by less CLCa incorporation in CCPs in cells with larger spreading areas, while not changing the number of clathrin triskelia. By immunostaining for alpha adaptin, a subunit of the integral CCP adaptor protein AP2, we verified that AP2 intensity was also lower with increasing cell spreading area (Supplemental Figure S1B), supporting the idea that cell spreading decreases the fluorescence

intensity of key endocytic components. Furthermore, we confirmed the decrease in CLCa fluorescence intensity in a different cell line with increasing cell spreading area (Supplemental Figure S1C). Together, these results show that CCP fluorescence intensity is lower with increasing the cell spreading area.

The decrease in CCP plateau intensity could arise from a slower clathrin polymerization rate or stalled clathrin polymerization at an earlier time, or a combination of the two. To differentiate between the two possibilities, the intensity profiles were examined and compared more closely. Figure 4A showed examples of overlay of the CCP intensity trajectory averaged over all CCPs for small and large cells for three different lifetime cohorts. While the time to reach the plateau intensity did not differ significantly (Figure 4B), the rate of CLCa intensity change was slower for cells on larger patterns (Figure 4C), showing that larger cell areas result in slower, and likely reduced, clathrin accumulation in CCPs.

Actin depolymerization and myosin contractility inhibition increase CCP fluorescence intensity

As the actin cytoskeleton and focal adhesions become more organized with increasing cell spreading areas on micropatterned substrates, we asked whether the mechanical property of cells changes in cells plated on patterned surfaces. To establish that cell spreading on patterned substrates modified cell tension, we examined the subcellular localization of recently identified transcription factors YAP (Yes-associated protein) and TAZ (transcriptional co-activator with PDZ-binding motif) that exhibit nuclear localization when cell tension is increased³³. Consistent with previous findings, immunostaining of YAP showed nuclear localization in larger cells; whereas YAP in small cells was found diffused in the cytosol (Supplemental Figure S2A). Further quantification revealed that only ~20% of 625 μm^2 square cells had nuclear localization of YAP compared to ~90% for 2500 μm^2 cells (Supplemental Figure S2B). This indicated that larger cells developed more tension than smaller cells. As

additional verification that cell tension increased with increasing cell spreading area, we employed micropipette aspiration to qualitatively measure the tension of the patterned cells as it reveals the force needed to deform the cell against a surface tension³⁴. Applying a negative pressure of 1.2 kPa and measuring the projection length of the plasma membrane within the pipette (L_p) and pipette diameter (D_p), we calculated the normalized projection length (L_p/D_p) to qualitatively compare cortical tension (Supplemental Figure S2C). A longer normalized projection length indicated lower cortical tension. The normalized projection length for 625 μm^2 cells was more than three times longer than for 2500 μm^2 cells (13.8 compared to 3.3) (Supplemental Figure S2D). Altogether, our results indicated that resting cell tension increased with cell spreading.

Since larger cells also had a more developed actin cytoskeleton as evidenced by more stress fibers (Figure 1 and 2) and developed more tension (Supplemental Figure SA), we next sought to examine how the actin network was related to CCP dynamics on micropatterned substrates. Treatment with a low dose of latrunculin A (LatA), which sequesters actin monomers, caused some reduction in actin stress fiber evident by fluorescence staining of actin filaments (Figure 5A). Under this condition, the proportion of short-lived CCPs increased significantly, especially for cells with the largest cell spreading area (Figure 5 B). Initiation density was similar before and after LatA treatment (Figure 5C), suggesting that mild disruption of actin network does not affect CCP initiation and that factors other than only tension affect CCP lifetimes and initiation density. Interestingly, the plateau fluorescence intensity of CCPs significantly increased with LatA treatment though it was not immediately clear why this occurred.

Finally, since the cortical actin network that is juxtaposed to the plasma membrane exerts cortical tension on the membrane via activity of motor proteins such as myosin, we wanted to test the hypothesis that cortical tension regulates the fluorescence intensity of CLCa in CCPs. Using another pharmacological inhibitor, Y-27632, that blocks the Rho-associated kinase ROCK and reduces myosin contractility, we observed that CCP intensity substantially

increased (Figure 5E). These experiments show that disrupting the actin cytoskeleton in larger cells results in more abortive CCPs with more clathrin fluorescence and that disrupting contractility also increased clathrin fluorescence in CCPs.

DISCUSSION

The structural context of a cell is important for understanding how cells sense and respond to physical and mechanical cues³⁵, and microcontact printing has been widely used to precisely control the degree of cell spreading^{19, 20, 36, 37}. Based on soft-lithography, the technique enables engineering of cellular microenvironment and can be used to generate carbohydrate, peptide and protein arrays³⁸. These microfabricated environments can be used to study structure and function of single cells, as in this study, or collective cell behaviors³⁹. Moreover, a variety of shapes can be made to control cell shape that guide distinct anisotropic internal cellular organization⁴⁰. The ability to control cell size or subcellular adhesion using microcontact printing is broadly applicable to other areas of cell and developmental biology, including cell organization, cell-cell interaction, cytoskeleton dynamics, cell adhesion, membrane trafficking, cellular differentiation....etc.

Here, we combined microcontact printing with quantitative live cell imaging of CCP dynamics and found that the proportion of short-lived CCPs and CCP intensity increased with large cell spreading area. CCP lifetimes range widely from under ten seconds to a couple of minutes^{8, 28}. Recently, several groups have shown that short-lived events under 20 s may represent failed dynamin 2 recruitment to CCPs^{24, 29-31}, which is required for vesicle scission, further demonstrating the abortive nature of short-lived CCPs. One evidence from our data supporting this classification of abortive CCPs is that CCPs with lifetimes less than 20s did not reach the maximum intensity attained by CCPs with > 40s lifetimes, suggesting incomplete assembly. Thus, one interpretation of our result is that increasing cell spreading area on micropatterned substrates increases the frequency of abortive CCPs as well as initiation density.

These two opposing effects would seem counterintuitive, and we speculate that in this case, a higher frequency of initiation could be coupled to the increase in abortive CCPs due to the larger a cytosolic pool of endocytic proteins arising from more frequent CCP disassembly. This could be understood as a mechanism to compensate for the increase in abortive CCPs to ensure the robustness of CME.

From our intensity analysis of CCP trajectories, we quantified maximum fluorescence intensity in cohorts of CCPs that had different lifetimes. Although CCPs are diffraction-limited, fluorescence intensity is proportional to the number of photons captured. In TIRF microscopy, the excitation intensity decays exponentially with the distance from the coverslip, so a dimmer signal could be due to the intrinsic property of TIRF imaging. However, our confocal imaging that had a ~500 nm depth of focus verified a similar result that CCP intensity was lower in cells with large cell spreading areas. Furthermore, the higher cortical tension as well as stronger adhesion in large cells would reduce the spacing between the coverslip and the membrane, and thus increase the fluorescence intensity instead of the observed decrease in fluorescence intensity. Finally, our analysis that included thousands of CCPs per cohort group would average out a distribution of different CCP shapes (if they exist). The correlation between plateau intensity and CCP size has been shown previously and used as an indicator for CCP size^{2, 41, 42}. Thus, one interpretation of fluorescence intensity is CCP size. It is possible that clathrin triskelia density in a CCP could change due to tension, though we think this possibility is low given the significant fluorescence intensity drop we observed. Although it remains a possibility that there could be very different CCP shapes that resulted in the changes in fluorescence intensity, we believe based on these considerations that a decrease in CCP intensity most likely results from a decrease in the number of clathrin triskelia, hence a decrease in CCP size. The slower clathrin accumulation rate could be due to the larger cell volume though cell heights also decreased with increasing cell area thereby increasing the effective concentrations that could not explain the slower polymerization rate (Supplemental Figure S3).

Using a dynamic growth model similar to what has been used previously to study focal adhesion assembly⁴³, we could gain additional insight on how clathrin polymerization rate changed with cell spreading area. Assuming the initial growth of a CCP is a flat domain where growth of the domain occurs only at the edge, but clathrin detachment can occur everywhere inside the domain with on- and off-rates as k_{on} and k_{off} , we have the dynamic equation for domain area as $\frac{dr^2}{dt} = k_{on}r - k_{off}r^2$. The rate of growth during early lifetime (i.e. r is small) yields $\frac{dr}{dt} \approx \frac{k_{on}}{2}$, with a steady state size $r_{ss} \approx \frac{k_{on}}{k_{off}}$. Since we found that increasing cell spreading area decreased the steady state sizes of CCPs by decreasing the rate of CCP growth, our dynamic growth model suggests a smaller k_{on} to satisfy these conditions.

Although we have found that cell tension increases with increasing cell spreading on our micropatterned substrates, there are likely biochemical and other biophysical changes between small and large spreading cells. For instance, focal adhesion signaling, cytoskeleton organization, and differences in protein expression could affect CCP dynamics. In our study, we used acute drug perturbations by LatA or Y-27632 just prior to imaging CCP dynamics. During this time period, gene expression profiles would unlikely change significantly, supporting the idea that a physical effect could be relevant here. However, we cannot exclude the possibility that changes in signaling or other non-specific effects of LatA or Y-27632 have on membrane trafficking could account for our findings. Since actin polymerization is essential for CCP invagination under high tension conditions¹⁷, our finding that the fraction of short-lived CCPs increased in cells treated with LatA on large patterns is consistent with the previous result.

Previous works have identified the importance of membrane tension in regulating certain aspects of CCP dynamics and the requirement of dynamic actin assembly in yeast and mammalian cells^{15,17}. The formation of coated vesicle is a balance of the energetic cost and energetic drivers, each of which are influenced by several parameters⁴⁴. In a theoretical study, the size of the vesicles can be influenced by tension through engaging actin polymerization and

where the actin forces act would determine the size of the vesicles⁴⁵. Using giant unilamellar vesicle as a model system and a theoretical framework to estimate polymerization energy from experimental data, it was found that there is a balance between membrane tension and polymerization energy that sets the shape of clathrin coats⁴⁶. Our work is consistent with the findings of both of these works. In eukaryotic cells, CCPs invaginate in the presence of a cortical actin network. Thus, endocytosis of CCPs requires deformation of the membrane that couples tightly to the cortical actin network where membrane mechanics should be considered as a membrane-cortex composite⁴⁷. In this context, it remains unclear what roles cortical actin network play in regulating distinct aspects of CCP dynamics since there is no clear relationship between cortical tension and membrane tension though it has been suggested that cortical tension has a huge influence on membrane tension⁴⁸. In our study, reduction in cortical tension by inhibiting myosin contractility resulted in lower CCP intensity (i.e. smaller CCPs). One way to conceptualize this is that the tension from stress-stiffening of the cortical actin network provides physical constraints⁴⁹, or effectively compressive forces, that limit the assembly of CCPs.

Membrane and cortex mechanics change actively as cells change shape during different cellular activities^{48, 50}. The shutdown of CME during early mitosis, presumably due to higher membrane tension, could be restarted by allowing actin to engage in endocytosis⁵¹. Additionally, several recent studies have highlighted the role of tension in cell migration^{52, 53, 54}, and how the tension gradient in motile cell could be coupled to polarized exo- and endocytosis⁵⁵. Although the functional significance of distinct CCP dynamics is not completely understood, it is becoming appreciated that endocytosis regulate signaling circuits by resolving signals in space and time⁵⁶. The ability of clathrin-coated structures to respond to physical cues agrees with the view that CME is not only a process of eating and drinking, but a process that is modulated according to a cell's physiological states. It requires further efforts to unravel the physiological meaning behind these modulation and adaptations to ensure the robustness of CME.

Acknowledgements

We thank Weiqiang Chen for fabricating the silicon master and Francois Aguet for help in data analysis. We acknowledge Sandy Schmid, Nir Gov, Kinneret Keren, Jeanne Stachowiak, Sapun Parekh, Yue Shao, and all members in Liu Lab for helpful discussions.

REFERENCE

1. H. T. McMahon and E. Boucrot, *Nat Rev Mol Cell Biol*, 2011, **12**, 517-533.
2. M. Ehrlich, W. Boll, A. van Oijen, R. Hariharan, K. Chandran, M. L. Nibert and T. Kirchhausen, *Cell*, 2004, **118**, 591-605.
3. M. A. Puthenveedu and M. von Zastrow, *Cell*, 2006, **127**, 113-124.
4. J. Z. Rappoport, S. Kemal, A. Benmerah and S. M. Simon, *American journal of physiology. Cell physiology*, 2006, **291**, C1072-1081.
5. A. P. Liu, D. Loerke, S. L. Schmid and G. Danuser, *Biophys J*, 2009, **97**, 1038-1047.
6. F. Nakatsu, R. M. Perera, L. Lucast, R. Zoncu, J. Domin, F. B. Gertler, D. Toomre and P. De Camilli, *J Cell Biol*, 2010, **190**, 307-315.
7. A. Grassart, A. T. Cheng, S. H. Hong, F. Zhang, N. Zenzer, Y. Feng, D. M. Briner, G. D. Davis, D. Malkov and D. G. Drubin, *J Cell Biol*, 2014, **205**, 721-735.
8. M. J. Taylor, D. Perrais and C. J. Merrifield, *Plos Biol*, 2011, **9**.
9. D. Nunez, C. Antonescu, M. Mettlen, A. Liu, S. L. Schmid, D. Loerke and G. Danuser, *Traffic*, 2011, **12**, 1868-1878.
10. A. P. Liu, F. Aguet, G. Danuser and S. L. Schmid, *J Cell Biol*, 2010, **191**, 1381-1393.
11. J. Dai and M. P. Sheetz, *Cold Spring Harbor Symposia on Quantitative Biology*, 1995, **60**, 567-571.
12. N. C. Gauthier, M. A. Fardin, P. Roca-Cusachs and M. P. Sheetz, *P Natl Acad Sci USA*, 2011, **108**, 14467-14472.
13. G. Warren, J. Davoust and A. Cockcroft, *Embo J*, 1984, **3**, 2217-2225.
14. B. Sinha, D. Koster, R. Ruez, P. Gonnord, M. Bastiani, D. Abankwa, R. V. Stan, G. Butler-Browne, B. Védie, L. Johannes, N. Morone, R. G. Parton, G. Raposo, P. Sens, C. Lamaze and P. Nassoy, *Cell*, 2011, **144**, 402-413.
15. S. Aghamohammadzadeh and K. R. Ayscough, *Nat Cell Biol*, 2009, **11**, 1039-1042.
16. L. M. Fujimoto, R. Roth, J. E. Heuser and S. L. Schmid, *Traffic*, 2000, **1**, 161-171.
17. S. Boulant, C. Kural, J. C. Zeeh, F. Ubelmann and T. Kirchhausen, *Nature Cell Biology*, 2011, **13**, 1124-U1158.
18. A. P. Liu, D. Loerke, S. L. Schmid and G. Danuser, *Biophysical journal*, 2009, **97**, 1038-1047.
19. C. S. Chen, M. Mrksich, S. Huang, G. M. Whitesides and D. E. Ingber, *Science*, 1997, **276**, 1425-1428.
20. R. McBeath, D. M. Pirone, C. M. Nelson, K. Bhadriraju and C. S. Chen, *Dev Cell*, 2004, **6**, 483-495.
21. F. Aguet, C. N. Antonescu, M. Mettlen, S. L. Schmid and G. Danuser, *Dev Cell*, 2013, **26**, 279-291.
22. W. Q. Chen, R. H. W. Lam and J. P. Fu, *Lab Chip*, 2012, **12**, 391-395.
23. Y. Iwadate and S. Yumura, *BioTechniques*, 2008, **44**, 739-750.
24. F. Aguet, C. N. Antonescu, M. Mettlen, S. L. Schmid and G. Danuser, *Dev Cell*, 2013, **26**, 279-291.
25. M. Mettlen, D. Loerke, D. Yarar, G. Danuser and S. L. Schmid, *Journal of Cell Biology*, 2010, **188**, 919-933.
26. J. L. Tan, J. Tien, D. M. Pirone, D. S. Gray, K. Bhadriraju and C. S. Chen, *P Natl Acad Sci USA*, 2003, **100**, 1484-1489.
27. K. Jaqaman, D. Loerke, M. Mettlen, H. Kuwata, S. Grinstein, S. L. Schmid and G. Danuser, *Nat Methods*, 2008, **5**, 695-702.
28. D. Loerke, M. Mettlen, D. Yarar, K. Jaqaman, H. Jaqaman, G. Danuser and S. L. Schmid, *Plos Biol*, 2009, **7**, 628-639.
29. M. J. Taylor, M. Lampe and C. J. Merrifield, *Plos Biol*, 2012, **10**, e1001302.
30. A. Grassart, A. T. Cheng, S. H. Hong, F. Zhang, N. Zenzer, Y. Feng, D. M. Briner, G. D. Davis, D. Malkov and D. G. Drubin, *J Cell Biol*, 2014, **205**, 721-735.
31. E. Cocucci, R. Gaudin and T. Kirchhausen, *Mol Biol Cell*, 2014, **25**, 3595-3609.

32. F. Huang, A. Khvorova, W. Marshall and A. Sorkin, *J Biol Chem*, 2004, **279**, 16657-16661.
33. S. Dupont, L. Morsut, M. Aragona, E. Enzo, S. Giulitti, M. Cordenonsi, F. Zanconato, J. Le Digabel, M. Forcato, S. Bicciato, N. Elvassore and S. Piccolo, *Nature*, 2011, **474**, 179-U212.
34. R. M. Hochmuth, *J Biomech*, 2000, **33**, 15-22.
35. D. E. Ingber, *Faseb J*, 2006, **20**, 811-827.
36. A. Kita, Y. Sakurai, D. R. Myers, R. Rounsevell, J. N. Huang, T. J. Seok, K. Yu, M. C. Wu, D. A. Fletcher and W. A. Lam, *PLoS One*, 2011, **6**, e26437.
37. Y. Shao, J. M. Mann, W. Chen and J. Fu, *Integr Biol (Camb)*, 2014, **6**, 300-311.
38. J. Voskuhl, J. Brinkmann and P. Jonkheijm, *Curr Opin Chem Biol*, 2014, **18**, 1-7.
39. S. R. Vedula, A. Ravasio, E. Anon, T. Chen, G. Peyret, M. Ashraf and B. Ladoux, *Methods Cell Biol*, 2014, **120**, 235-252.
40. M. Thery, V. Racine, M. Piel, A. Pepin, A. Dimitrov, Y. Chen, J. B. Sibarita and M. Bornens, *Proc Natl Acad Sci U S A*, 2006, **103**, 19771-19776.
41. C. N. Antonescu, F. Aguet, G. Danuser and S. L. Schmid, *Mol Biol Cell*, 2011, **22**, 2588-2600.
42. S. Saffarian, E. Cocucci and T. Kirchhausen, *Plos Biology*, 2009, **7**.
43. N. S. Gov, *Biophys J*, 2006, **91**, 2844-2847.
44. J. C. Stachowiak, F. M. Brodsky and E. A. Miller, *Nat Cell Biol*, 2013, **15**, 1019-1027.
45. N. Walani, J. Torres and A. Agrawal, *Proc Natl Acad Sci U S A*, 2015, **112**, E1423-1432.
46. M. Saleem, S. Morlot, A. Hohendahl, J. Manzi, M. Lenz and A. Roux, *Nat Commun*, 2015, **6**, 6249.
47. T. Z. Luo, K. Mohan, P. A. Iglesias and D. N. Robinson, *Nat Mater*, 2013, **12**, 1063-1070.
48. N. C. Gauthier, T. A. Masters and M. P. Sheetz, *Trends in Cell Biology*, 2012, **22**, 527-535.
49. J. Stricker, T. Falzone and M. L. Gardel, *J Biomech*, 2010, **43**, 9-14.
50. G. Salbreux, G. Charras and E. Paluch, *Trends Cell Biol*, 2012, **22**, 536-545.
51. S. Kaur, A. B. Fielding, G. Gassner, N. J. Carter and S. J. Royle, *eLife*, 2014, **3**, e00829.
52. A. R. Houk, A. Jilkine, C. O. Mejean, R. Boltyanskiy, E. R. Dufresne, S. B. Angenent, S. J. Altschuler, L. F. Wu and O. D. Weiner, *Cell*, 2012, **148**, 175-188.
53. A. D. Lieber, S. Yehudai-Resheff, E. L. Barnhart, J. A. Theriot and K. Keren, *Curr Biol*, 2013, **23**, 1409-1417.
54. A. D. Lieber, Y. Schweitzer, M. M. Kozlov and K. Keren, *Biophys J*, 2015, **108**, 1599-1603.
55. B. Fogelson and A. Mogilner, *PloS one*, 2014, **9**, e84524.
56. G. Scita and P. P. Di Fiore, *Nature*, 2010, **463**, 464-473.

FIGURE LEGENDS

Figure 1. Lifetime distribution and initiation density of CCPs on three sized circular cells.

(A) A EGFP-CLC RPE cell spread on $1024 \mu\text{m}^2$ circular fibronectin pattern (left). It is visualized using phase contrast microscopy (middle) and CCPs can be observed by TIRF microscopy (right). Dashed line highlights the outline of the cell. (B) Laser scanning confocal images of CCP (green), actin (red), paxillin (magenta) and nucleus (blue) for $625 \mu\text{m}^2$, $1024 \mu\text{m}^2$ and $2500 \mu\text{m}^2$ circular cells. (C) Lifetime distribution of CCP for three sized cells. Cells were imaged for 10 min, but lifetime distribution up to 120 s is plotted. Statistical significance between the distributions was confirmed using Kolmogorov–Smirnov test with a confidence level 0.05. Inset: scatter plot of proportion of 10 s – 18 s CCPs of each cell for three groups. Mean \pm S.D. is presented in the figure. (D) Scatter plot of initiation density of CCP of each cell for three sized cells (please refer to Methods section on how initiation density is calculated). Mean \pm S.D. is also presented in the figure. For (C) and (D), $N = 14, 10, 10$, and $N_{\text{CCP}} = 4372, 8667, 29351$ for $625 \mu\text{m}^2$, $1024 \mu\text{m}^2$ and $2500 \mu\text{m}^2$ circular cells respectively. Student's t test is performed between groups and p values are indicated in the figures.

Figure 2. Lifetime distribution and initiation density of CCPs on three sized square cells.

A EGFP-CLCa RPE cell spread on the $1024 \mu\text{m}^2$ square fibronectin pattern (left), visualized by phase contrast (middle) and by TIR-FM for CCPs (right). Dotted lines represent outline of the cell. (B) Confocal fluorescence images of CCP (green), actin (red), and paxillin (magenta) for $625 \mu\text{m}^2$, $1024 \mu\text{m}^2$, $2500 \mu\text{m}^2$ square cells. (C) Lifetime distribution of CCP for three sized cells. Statistical significance between the distributions was confirmed using Kolmogorov–Smirnov test with a confidence level 0.05. Inset: Proportion of 10 s – 18 s CCPs of each cell for three groups. Mean \pm S.D. is presented in the figure. (D) Initiation density of CCP of each cell for three sized cells. Mean \pm S.D. is presented in the figure. For (C) and (D), $N = 21, 8, 10$ and $N_{\text{CCP}} = 7260, 5767, 32708$ for $625 \mu\text{m}^2$, $1024 \mu\text{m}^2$ and $2500 \mu\text{m}^2$ square cells respectively. Student's t test is performed between groups and p values are indicated in the figures.

Figure 3. CCP intensity profile is modulated by cell spreading area.

(A) Average clathrin intensity traces in six lifetime cohorts (10-18, 20-38, 40-58, 60-78, 80-98, and 100-120 s) of $625 \mu\text{m}^2$ (left), $1024 \mu\text{m}^2$ (middle), and $2500 \mu\text{m}^2$ (right) circular cells. Each trace is derived from all the cells in that specific group. The shaded colored bands represent the standard error. Please refer to Method section on how the intensity traces were obtained. Black dashed line indicates the maximum intensity level for $625 \mu\text{m}^2$ cells. (B) Average plateau intensity of cohort 4 (60-78s) for circular and square cells of different cell spreading area. Error bar represents standard error. $N = 14, 10, 10$ for $625 \mu\text{m}^2$, $1024 \mu\text{m}^2$, and $2500 \mu\text{m}^2$ for circular cells, $N = 21, 8, 10$ for $625 \mu\text{m}^2$, $1024 \mu\text{m}^2$ and $2500 \mu\text{m}^2$ for square cells. (C) Average plateau intensity of cohort 4 for freely spreading cells, which are divided into two groups based on their size, $< 1100 \mu\text{m}^2$ and $> 1100 \mu\text{m}^2$. Cell numbers for two groups are 21, 25 and the number of CCPs are 9158 and 42408, respectively. Student's t test is performed between groups and p value is indicated in the figures.

Figure 4. Decrease in plateau intensity is due to a decrease rate of intensity change.

(A) Comparison of average intensity traces between $625 \mu\text{m}^2$ and $2500 \mu\text{m}^2$ circular cells for cohort 3 (left), 4 (middle), and 5 (right). (B) Comparison of time to arrive plateau intensity for cohort 2 to 6 between $625 \mu\text{m}^2$ and $2500 \mu\text{m}^2$ circular cells. The time point was determined by the first time point that fluorescence intensity reaches 95% of the maximum fluorescence intensity in a cohort from Figure 3A. (C) Rate of intensity change of CLCa in CCPs for lifetime cohorts 2 – 6 for $625 \mu\text{m}^2$ and $2500 \mu\text{m}^2$ circular cells. $N = 14, 10, 10$ for $625 \mu\text{m}^2, 1024 \mu\text{m}^2,$ and $2500 \mu\text{m}^2$ circular cells. Student's t test is performed between groups and p values are indicated in the figures.

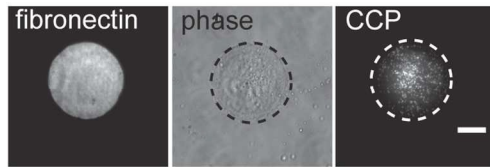
Figure 5. Latrunculin A and Y-27632 decrease CCP plateau intensity.

(A) Fluorescence images of cells after 20 minutes of 25 nM LatA treatment show that cells maintained their shapes, but with some visible changes to the actin cytoskeleton. (B) Proportion of short-lived (10 s to 18 s) CCPs for $625 \mu\text{m}^2$ and $2500 \mu\text{m}^2$ circular cells without and with 25 nM latrunculin A. $N = 14, 10$ and $N_{\text{CCP}} = 4372, 29351$ for $625 \mu\text{m}^2$ and $2500 \mu\text{m}^2$ circular cells without treatment. $N = 12, 13$ and $N_{\text{CCP}} = 4196, 48287$ for $625 \mu\text{m}^2$ and $2500 \mu\text{m}^2$ circular cells with 25 nM latrunculin A. Student's t test is performed between groups with the same size. (C) Initiation density for the same groups of cells in the Figure 2D. Wilcoxon rank sum test is performed between $625 \mu\text{m}^2$ groups because of the non-normality of the data. Student's t test is performed between $2500 \mu\text{m}^2$ groups. (D) Average plateau intensity of cohort 4 for $625 \mu\text{m}^2$ and $2500 \mu\text{m}^2$ circular cells with and without applying 25 nM latrunculin A. $N = 14, 10$ for $625 \mu\text{m}^2$ and $2500 \mu\text{m}^2$ circular cells without treatment. $N = 12, 13$ for $625 \mu\text{m}^2$ and $2500 \mu\text{m}^2$ circular cells with 25 nM latrunculin A. Student's t test is performed between groups and p values are indicated in the figures. (E) Average plateau intensity of cohort 4 for $625 \mu\text{m}^2, 1024 \mu\text{m}^2$ and $2500 \mu\text{m}^2$ circular cells with and without applying 3 μM Y-27632. $N = 14, 10, 10$ $N_{\text{CCP}} = 4372, 8667, 29351$ for $625 \mu\text{m}^2, 1024 \mu\text{m}^2$ and $2500 \mu\text{m}^2$ circular cells without treatment. $N = 10, 9, 8$ and $N_{\text{CCP}} = 3240, 7981, 43600$ for $625 \mu\text{m}^2, 1024 \mu\text{m}^2$ and $2500 \mu\text{m}^2$ circular cells with 3 μM Y-27632. Other cohorts had similar results.

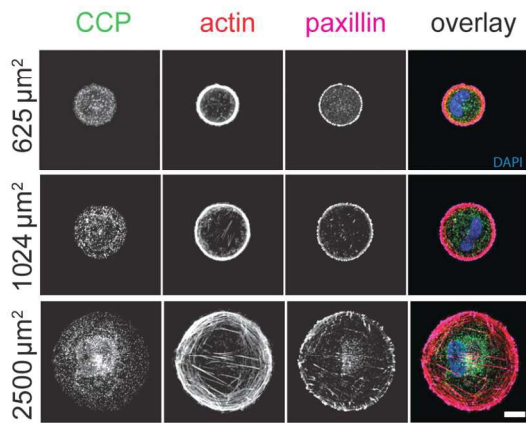
FIGURES

Figure 1

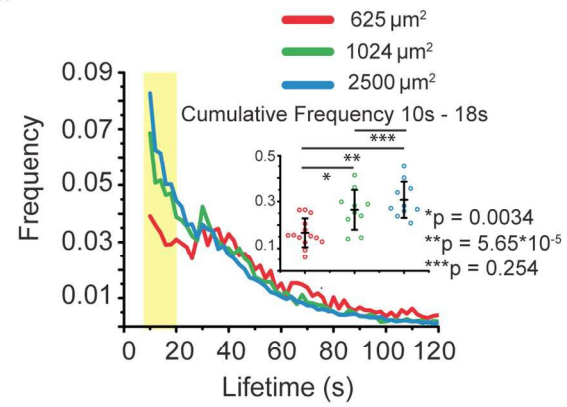
A.



B.



C.



D.

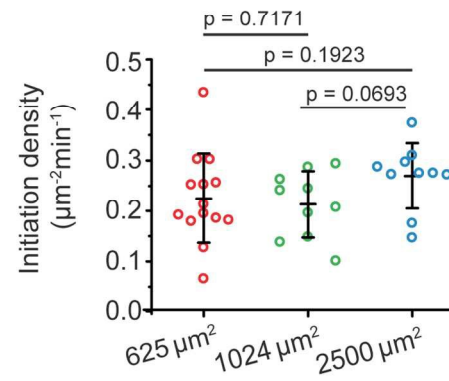


Figure 2

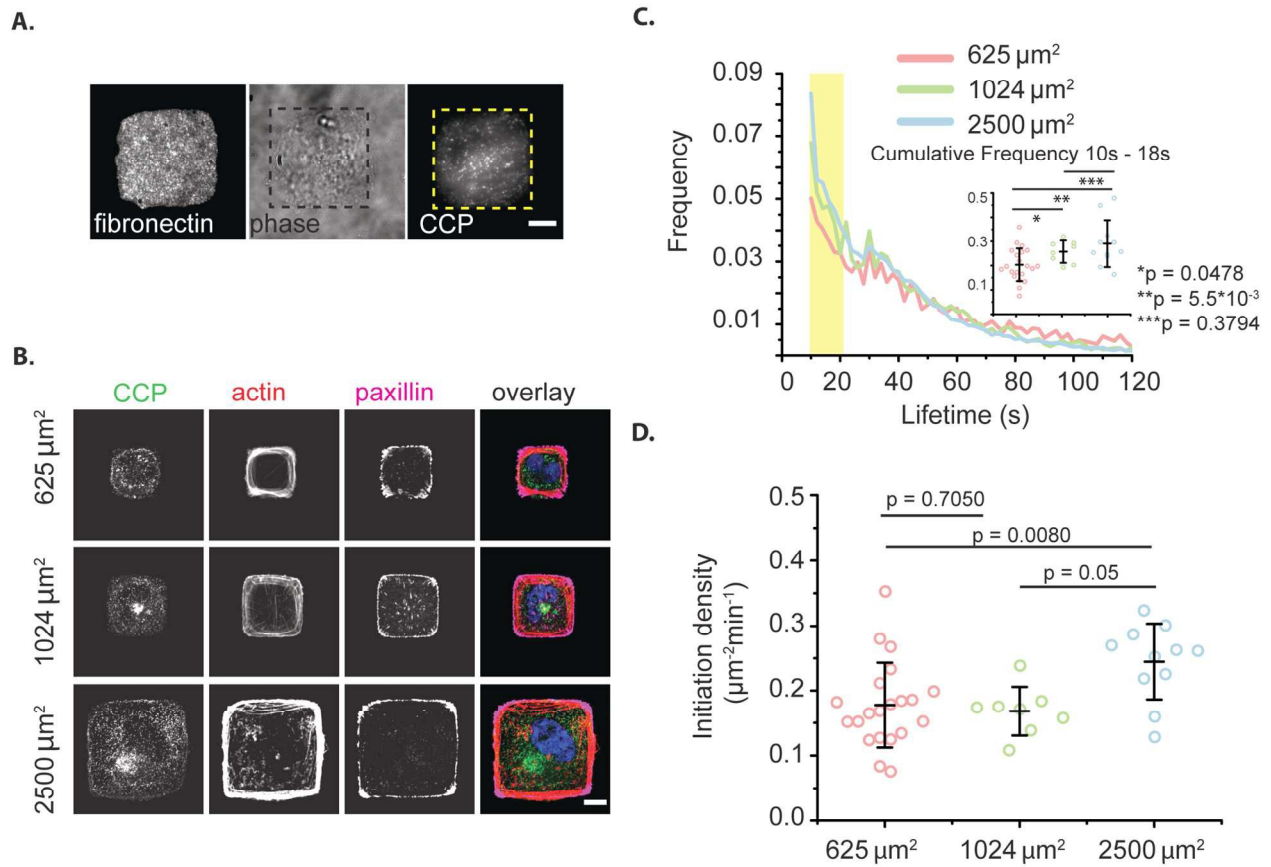


Figure 3

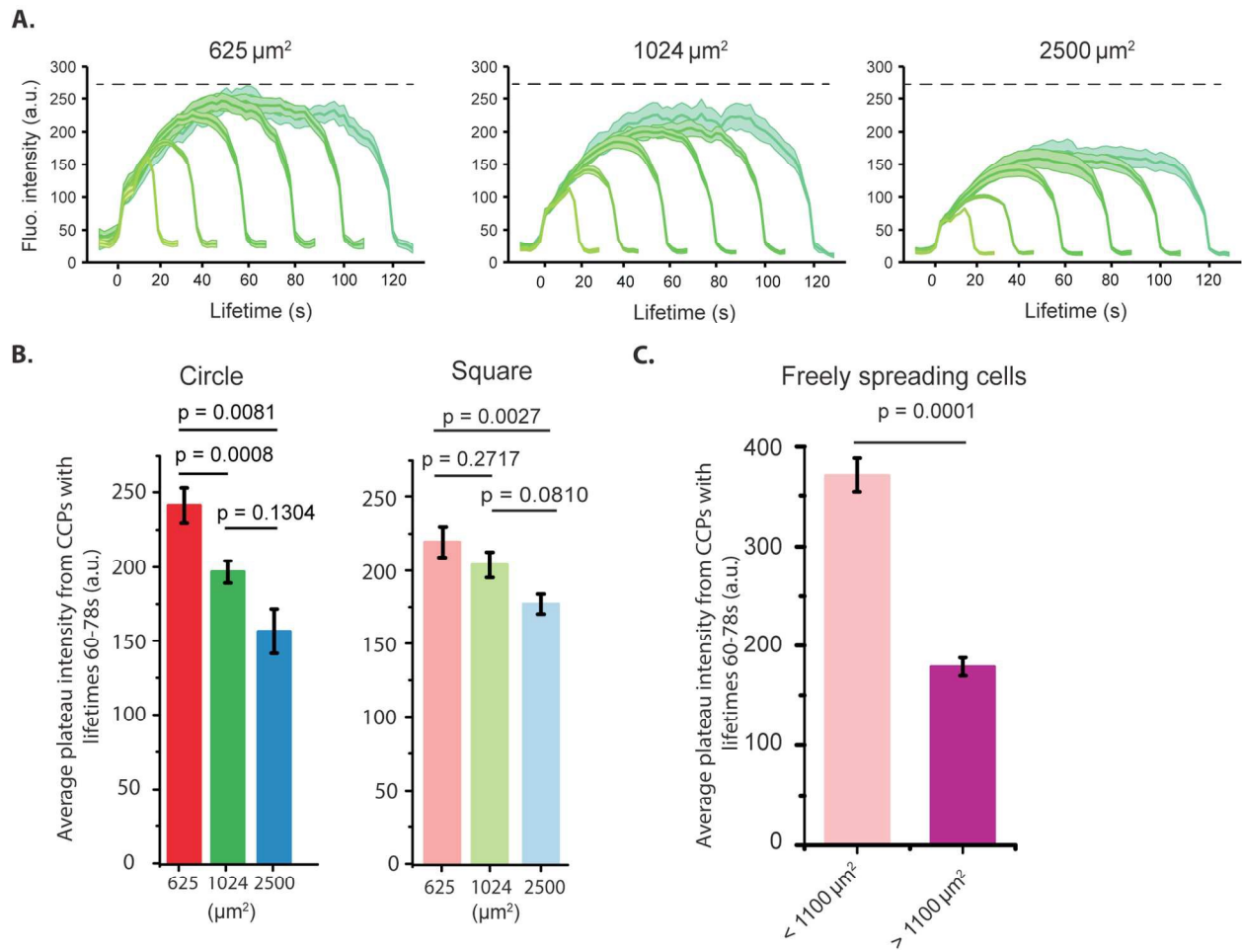
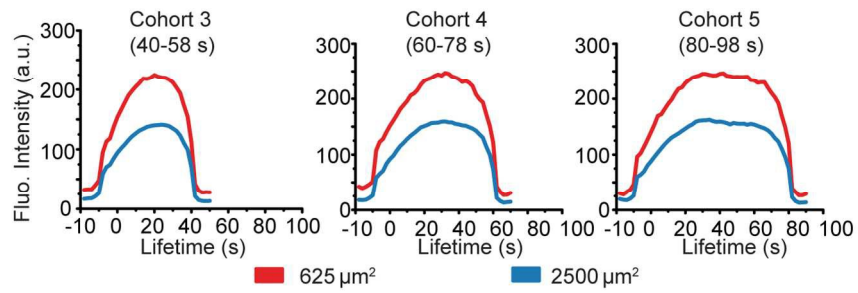
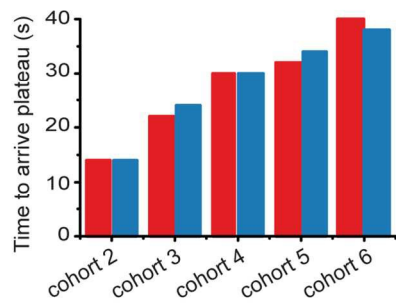


Figure 4

A.



B.



C.

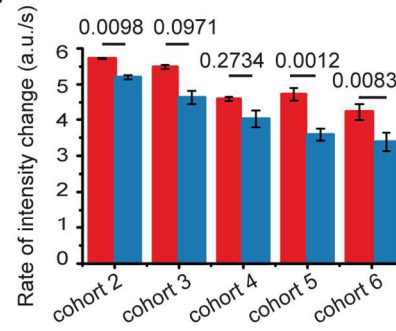
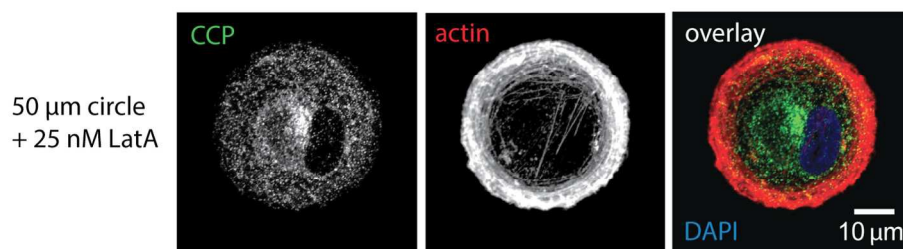
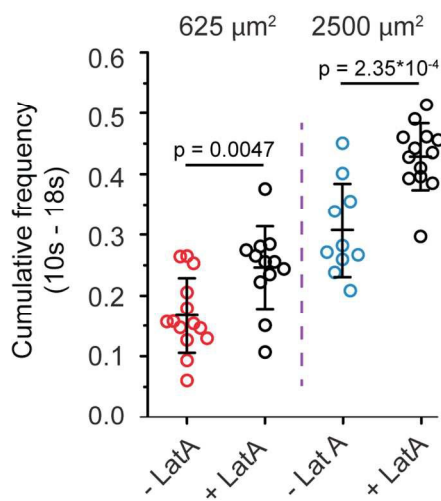


Figure 5

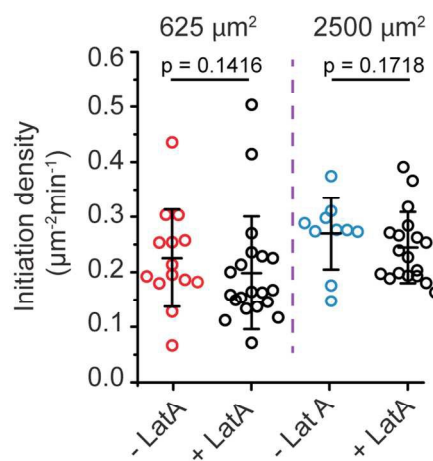
A.



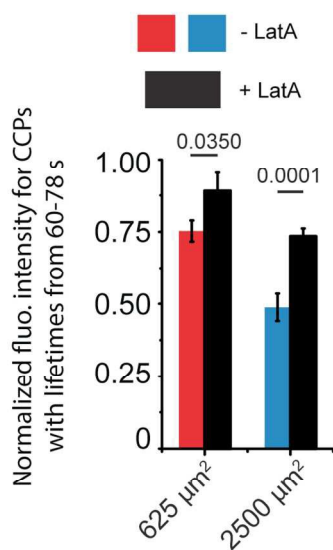
B.



C.



D.



E.

